Solar Energy Materials & Solar Cells 234 (2022) 111422

Contents lists available at ScienceDirect

Solar Energy Materials and Solar Cells

journal homepage: www.elsevier.com/locate/solmat

Novel coatings for graphite materials in PV silicon applications: A study of the surface wettability and interface interactions

Rania Hendawi *, Lars Arnberg, Marisa Di Sabatino

Department of Materials Science and Engineering, NTNU, 7491, Trondheim, Norway

ARTICLE INFO

Keywords:
Graphite
PV-Silicon
Phase-stability
Mechanism
Sustainability

ABSTRACT

Coatings are one of the promising techniques that can be applied to modify the surface properties and tailor the surface interactions with the surrounding. The development of conformable coatings for graphite materials can expand their use in silicon PV applications with no compromise on the silicon quality. However, no studies are focused on the coatings for graphite materials in silicon crystallization applications. Here we introduce different coating techniques that promise minimal interactions with the graphite and suppress the liquid silicon penetration. Five coating methods were proposed in this study: (i) one-layer coating: a mixture of silicon nitride and colloidal silica was directly coated on graphite substrates, (ii-iv) two-layer coating: a porous coating layer of silicon nitride, silicon carbide, or a combination of both materials was deposited as a protective layer below the top layer of Si_3N_4 and colloidal silica, and (v) a dense SiC layer was deposited on the graphite by silicon infiltration method below the top layer. The coatings' wettability and interactions with graphite were investigated via in-situ melting experiments. The two-layer coating approach revealed a considerable improvement in the non-wetting behavior, a decrease in the coating degradation rate, and a decrease in CO evolution during the isothermal holding. The best non-wetting conditions with minimal detrimental interaction between graphite and silicon oxides were achieved by applying a two-layer coating with a thickness of 400 ± 50 μm and an initial oxygen concentration of 8 wt.% in the top layer. These findings can be utilized for the application of reusable graphite crucibles in silicon crystallization processes.

1. Introduction

The need for an energy-efficient and environmental-friendly photovoltaic silicon production method has renewed the interest in the directional solidification route, which can be more sustainable by using reusable crucibles. Recently, two main alternatives of the single-use silica crucibles have been reported: graphite and silicon nitride crucibles [1–3]. While silicon nitride is chemically stable at high temperatures, its machinability and castability on alarge-scale can be challenging [4]. On the other hand, graphite is known for its good machinability and thermal durability, but it is highly reactive with silicon and silicon oxide at high temperatures. Therefore, the use of graphite crucibles in Si-casting applications requires a barrier coating layer that is poorly wetted by silicon and does not interact with graphite. Typically, in the case of silica crucibles, a high-purity silicon nitride coating layer is applied to facilitate the ingot removal and act as a diffusion barrier [5]. Silicon wetting of the coating layer is prevented by pre-oxidation of the silicon nitride coating that results in the formation of poorly wetted SiO_2 [6,7].

Most of the previous studies [8–12] on the graphite-silicon system have examined the wettability and the infiltration of silicon on bare (uncoated) graphite substrates. They have reported a rapid and complete wetting of the substrates followed by a formation of SiC as an intermediate layer. Only a few studies have attempted to investigate the wettability of silicon on coated graphite substrates [6,13]. Huguet et al. [13] have studied the wetting behavior of graphite samples that were coated with pre-oxidized silicon nitride powder at two different oxidation temperatures, namely 900 and 1100 °C. They have reported better non-wetting conditions at the high oxidation temperature. At isothermal holding, the silica content dissociates because of the reaction with the other system components. The major challenge, in this case, was the reduction of the SiO_2 by the graphite. It has been suggested that chemical vapor deposition of the SiC layer at the coating-substrate interface can act as a protective layer and prevent the SiO_2 reduction by the graphite.

Recently, Camel et al. [2] have documented successful pilot-scale

* Corresponding author.
E-mail address: rania.hendawi@ntnu.no (R. Hendawi).

https://doi.org/10.1016/j.solmat.2021.111422
Received 11 July 2021; Received in revised form 27 September 2021; Accepted 28 September 2021
Available online 26 October 2021

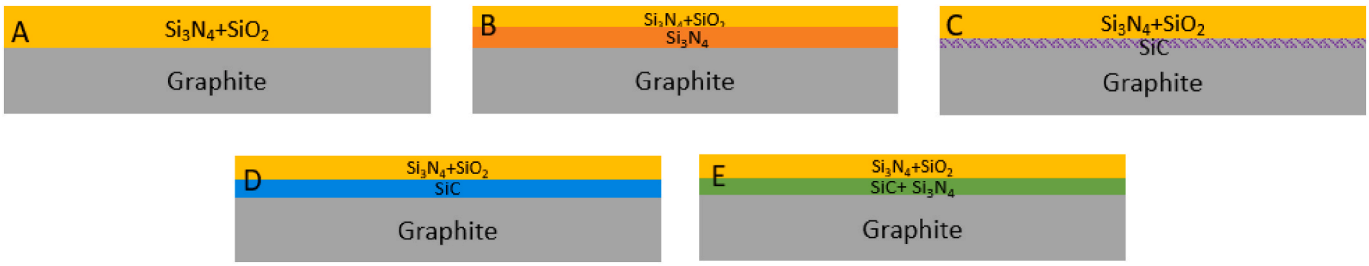

Fig. 1. Schematic of different coating configurations for graphite substrates. The top layer is the same for all configurations (Si_3N_4+SiO_2). The bottom layers in all methods are porous coating layers except for Coating-C that has a dense SiC layer as a bottom layer.

Table 1
Coating powder characteristics.

Characteristic	Si_3N_4	SiC	Si
Content	α-Si_3N_4 > 85%	β-SiC > 90%	–
Oxygen content	<1 wt.%	<1 wt.%	
Particle size	D98 < 7 μm D90 < 5 μm D50 < 2.2 μm	D50 = 6.5–8.5 μm	D50 = 5–8 μm

silicon ingot growth in graphite crucibles by using chemical vapor deposited (CVD) SiC layer at the coating-graphite interface. However, the high cost of CVD limits its feasibility for large-scale crucibles. This preliminary work on graphite crucibles has shown the need to examine different feasible coating approaches for better non-wetting conditions and the crucible's performance. A thorough investigation is needed for the possible interactions at (i) the graphite-coating interface and (ii) the coating-liquid silicon interface of all proposed coating methods.

In this work, we suggest different coating configurations that act as barrier layers and prevent silicon infiltration into graphite substrates. The major components of these coatings are silicon nitride, colloidal silica in addition to silicon carbide. The wetting properties and the chemical stability of the proposed configurations were examined via sessile drop experiments. Furthermore, the current study aims to systemically investigate the effect of oxygen concentration in the coating on its wetting properties. All the possible interactions at the interface of graphite-coating, coating-liquid, and their effects on the wetting behavior are discussed in detail.

2. Experimental

2.1. Coating preparations

Fig. 1 illustrates the five proposed coating configurations in this work. The top layer was prepared by a slurry composed of high purity Si_3N_4 powder, colloidal silica, and polyvinyl alcohol as a binder dispersed in deionized water. The main goal of the top layer is to achieve non-wetting conditions during melting as it will be in contact with liquid silicon. The oxygen mass concentration of this layer is controlled by addition of colloidal silica.

The bottom layer of the coatings acts as a protective layer of graphite substrates that suppress the contact between SiO_2 in the top layer and the graphite. To achieve this, four different alternatives were presented:

i. Porous silicon nitride coating layer prepared by mixing high purity silicon nitride powder with polyvinyl alcohol (PVA) as a binder dispersed in deionized water. (Coating-B)
ii. A dense silicon carbide layer was deposited by melting solar grade silicon powder over graphite substrates at 1450 °C in an argon atmosphere. (Coating-C)
iii. A porous silicon carbide layer was prepared by mixing SiC powder with PVA and deionized water. (Coating-D)
iv. A slurry of (1:1) powder mixture of silicon nitride and silicon carbide, PVA binder, and deionized water was sprayed on graphite substrates. (Coating-E)

All the slurries were sprayed by a 0.3 mm nozzle on the pre-heated

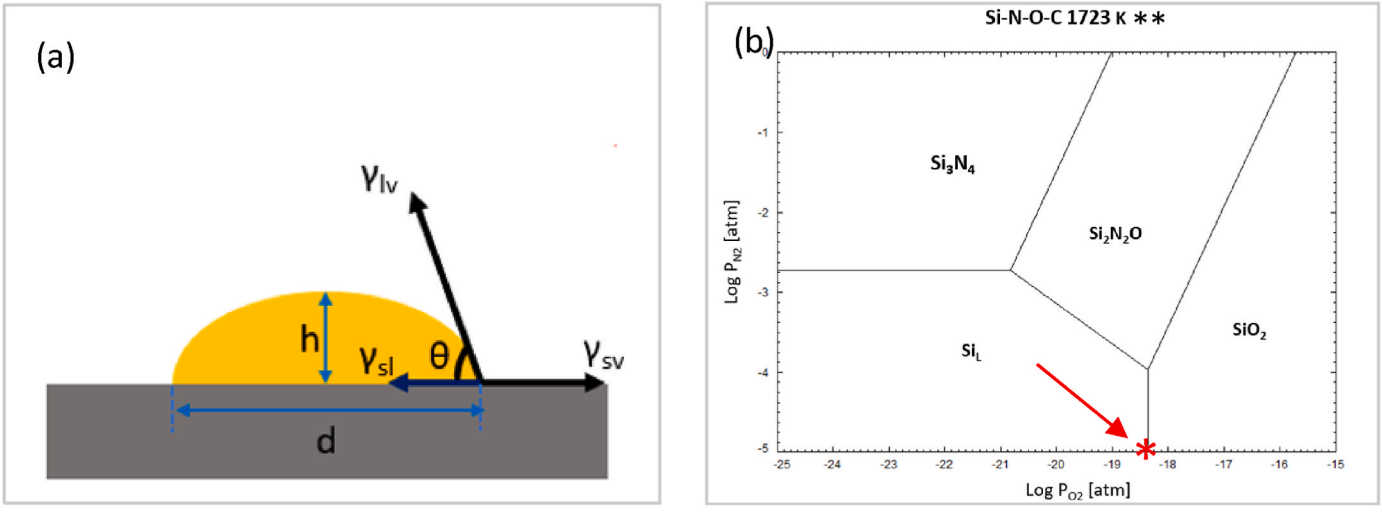

Fig. 2. (a) Schematic drawing of the sessile drop configuration showing the definition of the three measured parameters; θ: contact angle between the drop and the coating surface, h: the height of the droplet, and d: diameter of the droplet base. γ is the interfacial energy between solid, liquid, and vapor phases. (b) Phase diagram of Si–N–O–C system at $P_{CO} = 10^{-3.3}$atm.* The red arrow points at the critical oxygen partial pressure for the oxide-free Si droplet. ** Calculated by Factsage 8.1. (For interpretation of the references to color in this figure legend, the reader is referred to the Web version of this article.)

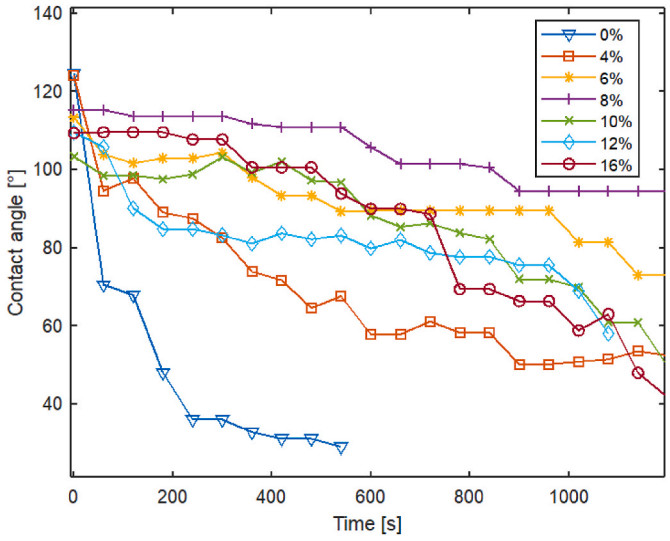

Fig. 3. Development of the contact angle at different initial oxygen concentrations of the coating type-B at 1723 K. The legend represents the initial oxygen mass concentration in the coating. The total coating thickness is 200 ± 30 μm (each layer is 100 ± 15 μm). (Second replicate is included in Supplementary materials Fig. S2.)

graphite substrates (10 × 10 × 5 mm^3) at 120 °C. The characteristics of the coating powder are given in Table 1. The thickness of the porous bottom layer in types A, B, D, and E is half of the total thickness. The thickness of the dense silicon carbide layer in type C ranges from 10 to 50 μm. The standard total thickness of the coating (including both layers) is 200 ± 30 μm. However, to study the effect of the coating thickness on the coating stability, thicker layers (up to 500 μm) are applied on some graphite substrates.

2.2. In-situ melting

In-situ melting experiments were performed in a graphite sessile drop furnace. The existence of graphite insulation is crucial to study the effect of the natural forming CO gas on the coating degradation and wetting process. As known, during silicon crystallization, CO gas is formed according to the following reaction:

$$SiO_g + 2C \leftrightarrow CO_g + SiC \quad (1)$$

The graphite furnace was equipped with a digital video camera (Sony XCD-SX910CR) to record the shape of the droplet during melting (10 frames per second). Three major parameters are measured during the isothermal holding as shown in Fig. 2: (i) the contact angle between the silicon droplet and the coating surface (θ) with an accuracy of ±2°, (ii) the diameter of the droplet base (d) and the height of the droplet (h) with an accuracy of ±4%. 100 mg solar-grade silicon samples (8 N purity) were placed on the coated graphite substrates and heated under vacuum (10^{-6} mbar) to 800 °C for degassing. Then argon gas (6 N purity) was introduced with a flow rate of 0.5 L/min during heating to 1450 °C. The oxygen level in the furnace was measured by a zirconia sensor that was attached to the gas outlet. The oxygen partial pressure in the furnace upon melting was 10^{-19} atm, which is crucial to avoid the formation of an oxide layer on the molten silicon drop as the critical oxygen partial pressure for oxide-free droplet is $10^{-18.5}$ atm (see Fig. 2 b). Two replicates were performed for each experiment to assure reproducibility. The run order of the experiments was randomized to eliminate the effect of any uncontrollable factors on the results.

2.3. Characterization

The morphology and structure of the samples were studied using a Zeiss Ultra 55 SEM. To investigate the interfaces of the coated samples after melting, Raman scanning was performed using a WITec alpha300-R instrument with a 532 nm laser. Raman spectra were obtained after 8 accumulations for 10 s from 50 to 3500 cm^{-1}.

Table 2
Contact angle data between silicon and different refractory materials as reported in the literature at 1430 °C in Ar.

Substrate	Equilibrium contact angle [°]	Ref.	Comments
Si_2N_2O	>95	[16]	
SiO_2	70–85	[6,13,17]	Wide range due to the variation in the surface roughness
Si_3N_4	45–50	[6,18]	

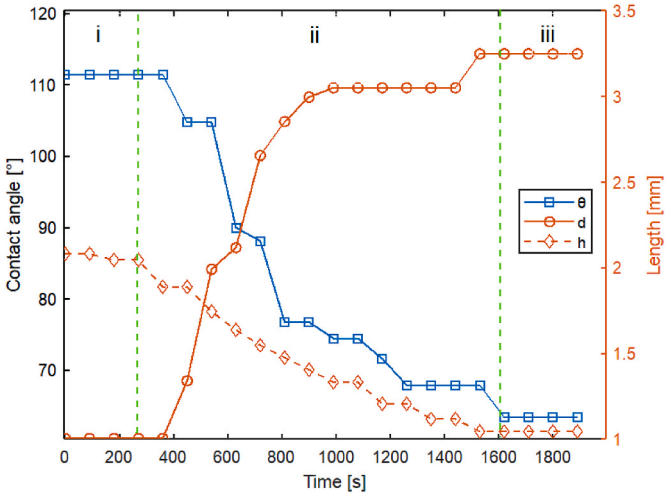

Fig. 4. Wetting curves for a two-layer (type-B) coated sample with an initial oxygen concentration of 8 wt.%. (i-iii) represent the wetting stages. θ: contact angle between the silicon droplet and coating surface, d: the diameter of the droplet base, and h: the height of the droplet. The total coating thickness is 200 ± 30 μm (each layer is 100 ± 15 μm). More examples of wetting curves are given in Supplementary materials. (For interpretation of the references to color in this figure legend, the reader is referred to the Web version of this article.)

3. Results and discussion

3.1. Wetting kinetics

Fig. 3 shows the wetting behavior of type-B coating at different oxygen concentrations of the top layer. The oxygen content was controlled by colloidal silica additions to the top layer of the coating as mentioned in detail in the experimental part. The oxygen content affects not only the wetting degree but also the wetting rate. Apparently, all the tested samples experienced a transition from non-wetting (θ > 90°) to wetting conditions (θ < 90°) at some point during the sessile drop experiments. Oxygen content in the range of 6–8 wt.% results in the lowest wetting rates of the substrates. However, increasing the oxygen content of the coating above 8 wt.% does not lead to any further improvement in the non-wetting conditions.

These observations lead to a question of the main product that is responsible for the de-wetting conditions. Table 2 lists the reported contact angles of silicon on different substrates in the literature. Comparing the reported equilibrium data in the literature with the measured contact angles at 8 wt.% suggests the formation of Si_2N_2O at the triple line (where solid, liquid, and gas phases coexist), which also agrees with our previously reported results [14]. The formation of silicon oxynitride at the triple line results from the reaction of the dissolved nitrogen and oxygen with molten silicon as follows:

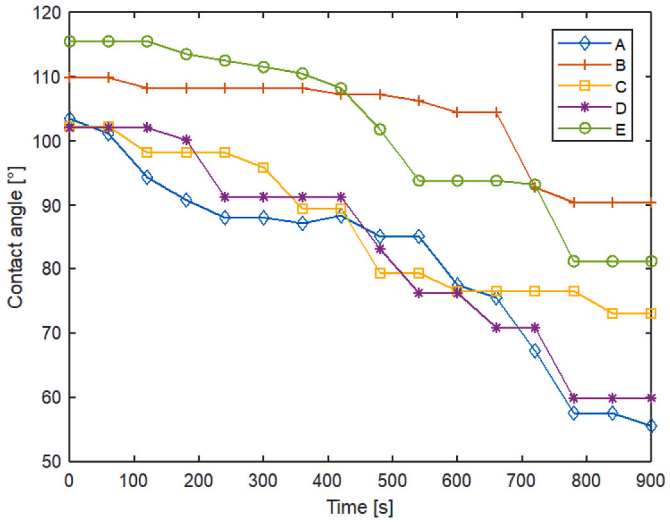

Fig. 5. Development of the contact angle at 1723 K as a function of time for different coating configurations. Details of the coatings are included in Fig. 1. The total coating thickness is 200 ± 30 μm (each layer is 100 ± 15 μm). The second replicate is included in Supplementary materials Fig. S2. Images of the coating microstructure of all samples are included in Supplementary materials (Fig. S4.).

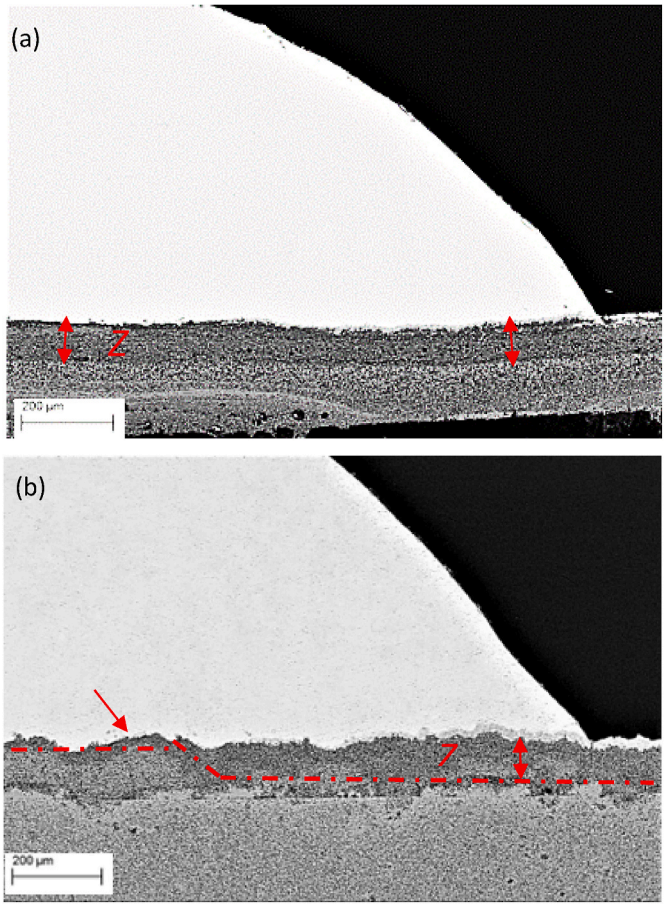

Fig. 6. The drop configuration and coating microstructure of two substrates; (a) type-A coated graphite substrate and (b) type-A coated silicon nitride substrate. The initial oxygen concentration of the coatings is 8 wt.%. The red dashed lines indicate the deoxidation depth of the coating. Z is the deoxidation depth of the coating (μm). (For interpretation of the references to color in this figure legend, the reader is referred to the Web version of this article.)

$$2Si_l + 2N_i + O_i \leftrightarrow Si_2N_2O \quad (2)$$

Nitrogen and oxygen are the main products of the coating degradation process. The moderate deoxidation rates of 8 wt.% oxygen content coating advance the formation of silicon oxynitride at the liquid front as shown in Ref. [14]. Fig. 4 illustrates an example of the wetting curves at 8 wt.% oxygen content for type B coated substrate. A continuous change in the drop geometry and the contact angle, which is so-called dynamic wetting, is noticed. The three stages of the dynamic wetting that were observed via the wetting experiments are summarized below:

i. An initial transient stage where the contact angle and the drop geometry remain constant.
ii. A decrease in the contact angle is accompanied by an increase in the drop base diameter and a decrease in the height of the drop, which indicates the spreading and infiltration of liquid silicon.
iii. Constant contact angle and drop parameters.

It is noticed that the liquid spreading, which is represented by a decrease in the contact angle accompanied with an increase in the drop base, precedes the liquid infiltration into the coating. The infiltration of liquid is characterized by a sharp decrease of the droplet height as proposed by Ref. [15] (see more examples in Supplementary materials). The liquid spreading rate can be identified by the change in the drop radius versus time. The main driving force of spreading is the dissociation of poorly wetted oxynitride compound at the triple line of the droplet as we showed in Ref. [14]. On the other hand, the liquid infiltration into the coating is driven by the dissociation of the poorly wetted products at the liquid front in the pores of the coating. The infiltration rate can be calculated by measuring the liquid infiltration depth (l) in the coating over time (see Fig. S3. in Supplementary materials). The careful examination of Fig. 4 suggests a high spreading rate compared to the infiltration rate, which also can be noticed in the images of the droplet configurations after sessile drop experiments (see Fig. 6). Thus, the dissociation of silicon oxynitride at the triple line is expected to be faster than at the liquid front under the droplet.

Fig. 5 shows the wetting behavior for the five coating types at 8 wt.% oxygen concentration. The two-layer coating types B and E show the lowest change in the contact angle over time. Slight differences in contact angle development over time are found between coating types A, C, and D. Since the top layer is the same for all coating configurations, the variation in the wetting behavior can be related to (i) the ongoing interactions at the graphite-coating interface and liquid-coating interface (ii) the coating strength and adhesion to the substrate, which will be discussed in detail in the next sections. It is worth noting that reactive wetting of coated substrates is a complex phenomenon that is affected by several factors. The wettability behavior of the proposed coating configurations can be an indication of the coating efficiency during the melting process of silicon but cannot reflect the overall picture. Therefore, in this work, the performance of all coating types is assessed based on: (i) the wetting curves, (ii) the examination of coating microstructure, (iii) the deoxidation of the coating during melting, and (v) the interactions with other system components. Further discussions are given in section 3.6.

3.2. Kinetics of oxygen depletion

The oxygen content of the coating depletes during the isothermal holding of the coated substrates at 1723 K because of SiO_2 dissociation. The depletion rate can be calculated by measuring the depleted (deoxidized) coating depth over time ($\frac{dZ}{dt}$) as illustrated in Fig. 6. The experimentally measured depletion rates for different coated substrates under the same melting conditions, holding temperature, and argon flow rate are shown in Fig. 7.a. Higher depletion rates are reported for graphite substrates compared with silicon nitride and quartz substrates. The obtained higher deoxidation values suggest a different depletion

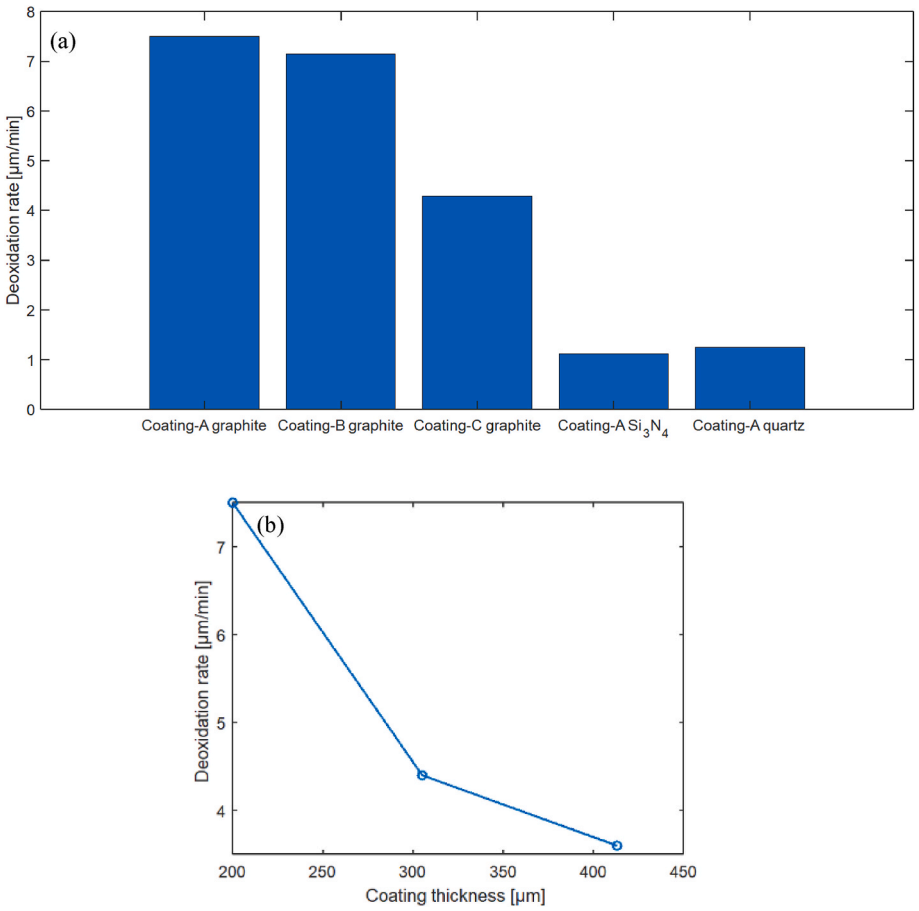

Fig. 7. (a) Experimentally calculated deoxidation rates of different coating techniques after in-situ melting of silicon at 1723 K (under the droplet). The total coating thickness is 200 ± 30 µm. (b) The deoxidation rate of coated graphite substrates (type-B) as a function of the total coating thickness. The initial oxygen concentration of the top layer is 8 wt.% in all coated substrates. (For interpretation of the references to color in this figure legend, the reader is referred to the Web version of this article.)

mechanism in the existence of the graphite substrates. The depletion process of the silica content in the coated graphite substrates is mainly driven by three major factors: (i) direct contact of the SiO_2 content in the coating with liquid Si, at the liquid-coating interface; (ii) self-reduction of SiO_2 by Si_3N_4 in the bulk of the coating; and (iii) reduction by interacting with graphite substrate at the coating-graphite interface. It should be noted that the effect of carbon vapor pressure on the reduction of SiO_2 is neglected at 1723 K [19].

To better understand the mechanism of the SiO_2 dissociation, Fig. 6 shows the coating microstructure after the in-situ melting experiments

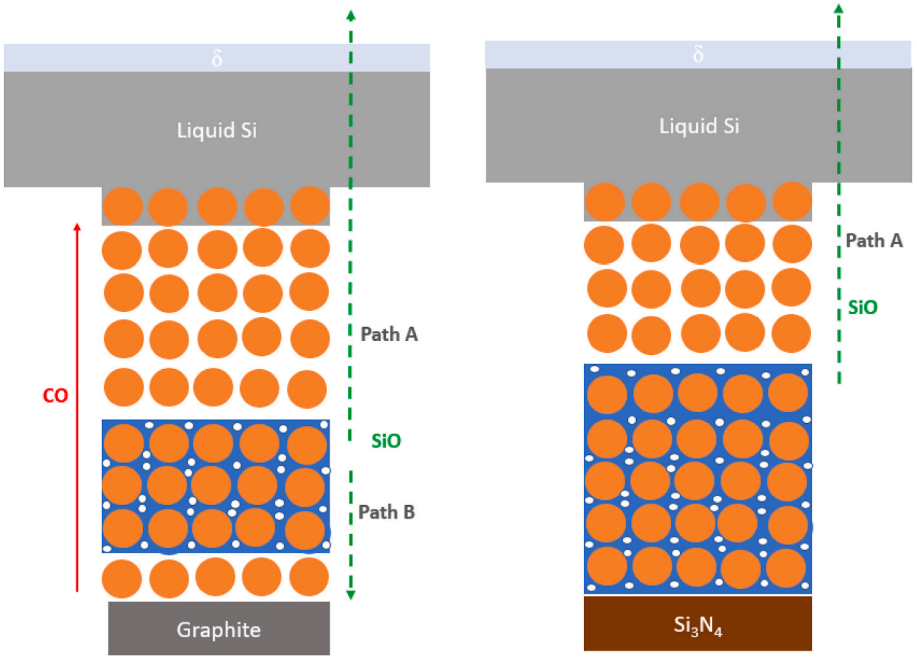

Fig. 8. Schematic drawing of the SiO path with two substrates; graphite (left) and silicon nitride (right). The orange color indicates Si_3N_4 particles, while the blue layer is silica. The main steps in path A are (i) diffusion of SiO in the remaining silica layer, (ii) diffusion in the porous coating, (iii) diffusion in the infiltrated coating, (iv) diffusion in the liquid, (v) diffusion in the gas boundary layer. Main steps in path B: (i) diffusion in the remaining silica layer, and (ii) diffusion in the porous coating. (For interpretation of the references to color in this figure legend, the reader is referred to the Web version of this article.)

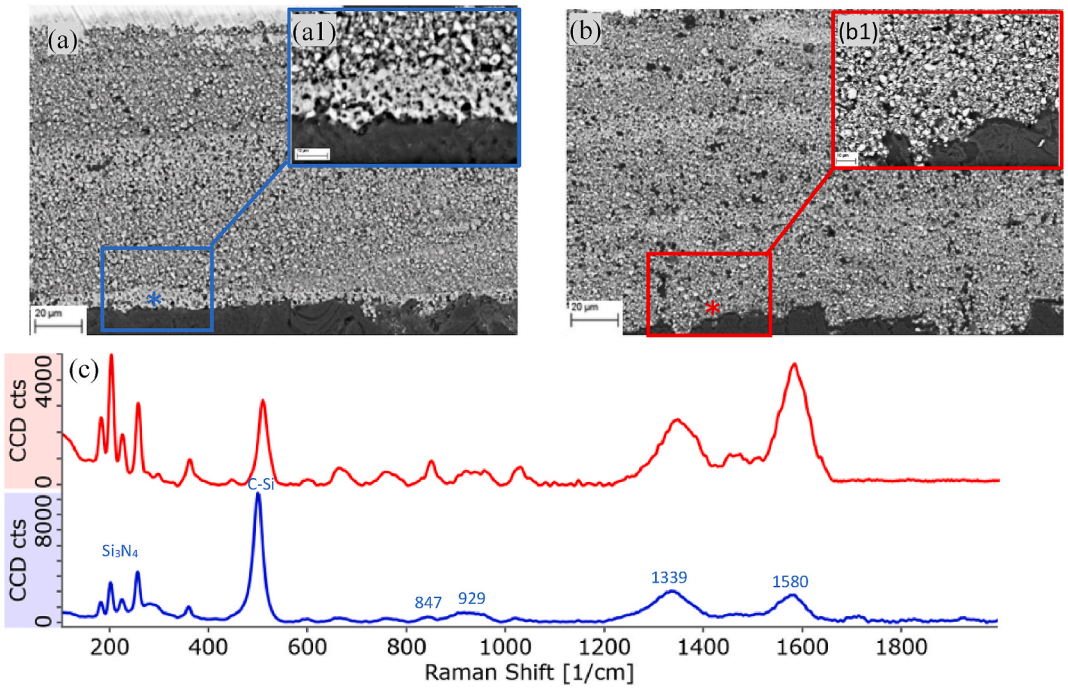

Fig. 9. (a) The one-layer coating microstructure after 30 min holding at 1723 K and high magnification of the coating-substrate interface (a1). (b) The two-layer type-B coating microstructure and a high magnification micrograph of the coating-substrate interface (b1). (c) The corresponding typical Raman spectra of the coating-graphite interface of (a1) in blue and (b1) in red. The initial oxygen concentration of the top coating layer of both samples is 8 wt.%. The total coating thickness is 200 ± 30 μm. The * corresponds to the points scanned by Raman. (For interpretation of the references to color in this figure legend, the reader is referred to the Web version of this article.)

for graphite and Si_3N_4 substrates. The silicon nitride substrate stands for a reference sample as it is an oxygen-free material and acts as inert material in the system. The coating depletion seems to start at the liquid-coating interface and proceeds toward the bulk of the coating. At the liquid-coating interface, SiO_2 dissolves in the molten silicon into oxygen and silicon. This transient stage is followed by the reduction of SiO_2 due to the reaction with silicon nitride particles, which results in SiO and nitrogen evolution. In the one-layer coated graphite samples, as there is a direct contact between SiO_2 and the graphite, SiO_2 also dissociates at the coating-substrate interface as shown in Fig. 6.a. The careful examination of the oxygen-depleted coating in Fig. 6.b reveals an anisotropic depletion behavior of the coating, which means that the depletion depth is inversely proportional to the liquid height (Z increases towards the triple line). This has been explained previously by considering that the SiO_2 dissociation, below the drop, is limited by the evacuation of the product gas, namely SiO, to the gas atmosphere [20]. It has been found that the slowest step in the evacuation path is the diffusion of oxygen in the liquid and, hence, the rate increases as the liquid height decreases towards the triple line [20].

On the other hand, this behavior is not noticed with graphite substrates as illustrated in Fig. 6.a. The deoxidized coating depth under the droplet does not change with the liquid height, which indicates that SiO_2 dissociation reaction is no longer limited by the oxygen diffusion in the liquid. With graphite substrates, there are two evacuation paths that SiO can follow: (i) diffusion towards the furnace atmosphere, and (ii) diffusion towards the graphite substrate as schematically illustrated in Fig. 8. SiO reacts with graphite and forms CO gas, which then evacuates to the gas atmosphere. The high deoxidation rates of coated graphite substrates compared with other materials are explained by this additional diffusion path of SiO, which acts as a driving force for the deoxidation. Therefore, the two SiO sinks in the system (the dynamic gas atmosphere and the graphite substrates) accelerate the oxygen depletion process. This suggests a crucial role of the coating thickness on the coating deoxidation since increasing the thickness of the coating will slow the diffusion of SiO gas to the graphite substrate and hence decrease the deoxidation rate as revealed in Fig. 7.b. As can be noticed in Fig. 7.b, applying a 400 μm of coating-B results in a low deoxidation rate that is similar to the type-C deoxidation rate. However, increasing the thickness over 500 μm leads to coating cracking as shown in Supplementary Materials Fig. S6

3.3. *Interactions at the coating-substrate interface*

Fig. 9 shows the coating-graphite interface of the one-layer and two-layer configurations. As shown in Fig. 9.a, the reaction between the graphite substrate and the coating components leads to a formation of an intermediate layer with a different microstructure than the other regions of the coating. Raman analysis in Fig. 9.c of this layer reveals a high crystal silicon peak (511 cm^{-1}), which suggests that the graphite reduces silica by:

$$SiO_2 + 2C \leftrightarrow Si_l + 2CO \quad (3)$$

The peaks at 849 and 929 cm^{-1} correspond to amorphous silicon carbide as suggested by Ref. [21]. The high carbon peaks (1339 and 1580 cm^{-1}) in this regime block the crystalline-SiC peaks [21]. Graphite can also reduce silica by the following reactions:

$$SiO_2 + C \leftrightarrow SiO + CO \quad (4)$$

$$SiO_2 + 3C \leftrightarrow SiC + 2CO \quad (5)$$

The examination of the coating-substrate interface in the two-layer coated samples (type-B) also suggests the existence of an amorphous SiC phase as shown by the red spectrum in Fig. 9.c. The responsible reaction of SiC formation in this case is:

$$Si_3N_4 + 3C \leftrightarrow 3SiC + 2N_2 \quad (6)$$

So, the SiC layer is formed by both coating methods. However, the key benefit of the two-layer coating is the formation of the SiC layer

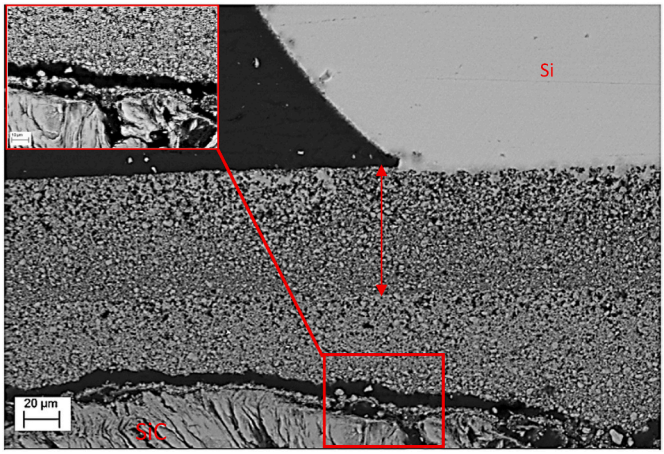

Fig. 10. The coating microstructure of type-C coating after sessile drop experiment 1450 °C. The red arrow denotes the deoxidized coating depth (Z). No deoxidation is found at the interface between SiC and the porous coating. (For interpretation of the references to color in this figure legend, the reader is referred to the Web version of this article.)

without the evolution of CO gas as in the other method as seen in Reaction 6. Another significant reaction that occurs at the graphite surface in both configurations (A and B) is the reaction between graphite and SiO gas that results from the deoxidation of SiO_2 in the bulk of the coating and diffusion through the porous coating to the substrate surface (see Reaction (1)). This reaction will also lead to silicon carbide formation by the gas-solid reaction. The resulting thickness of the silicon carbide layer (τ_{SiC}) can be estimated by the equations below:

$$\frac{dn_{SiC}}{dt} = A\left(k_f P_{SiO} a_C^2 - k_r P_{CO} a_{SiC}\right) \tag{7}$$

$$\tau_{SiC} = \frac{n_{SiC}}{\eta_{SiC} A} \tag{8}$$

n_{SiC} is the number of SiC moles formed by the gas-solid reaction. k_f and k_r are forward and reverse reaction rate constants [22]. The calculated values of k_f and k_r at 1723 K are 3.11×10^{-7} and 5.12×10^{-10} $mol/cm^2 s.atm$ respectively according to the following equations by Ref. [22]:

$$ln k_f \left(\frac{mol}{cm^2}.s.atm\right) = 29.175 - \frac{76083}{T} \tag{9}$$

$$ln\, k_r \left(\frac{mol}{cm^2}.s.atm\right) = 53.518 - \frac{129072}{T} \tag{10}$$

a_C and a_{SiC} are the graphite and silicon carbide activities, which are assumed to be unity. A is the reaction surface area (cm^2), which is the surface area of the graphite substrate. P_{SiO} is the partial pressure of SiO at the reaction surface, which is estimated to be the equilibrium partial pressure of SiO in the following reaction:

$$3SiO_2 + Si_3N_4 \leftrightarrow 6SiO + 2N_2 \tag{11}$$

η_{SiC} is the molar density of SiC (mol/cm^3). P_{CO} is the partial pressure of product gas CO. Since the reverse reaction rate is found to be three orders of magnitude less than the forward rate, the second term in equation (7) can be neglected especially that CO is continuously evacuated towards the gas atmosphere. The theoretical silicon carbide thickness that can be formed by the SiO-graphite reaction during 30 min of the isothermal holding 1723 K is 452 nm. It should be noted that this is the maximum hypothetical thickness that can be achieved via the solid-gas reaction if the partial pressure of SiO is at the equilibrium value. However, a departure from equilibrium results in a lower partial pressure of SiO and hence SiC thickness.

In coating type-C, the applied dense SiC layer prohibits the previously discussed interactions between graphite and Si_3N_4 and SiO_2. Regarding the possibility of silica reduction by SiC, in this case, Huguet et al. [13] has proposed this reaction:

$$2SiC + SiO_2 \leftrightarrow 3Si_l + 2CO \tag{12}$$

However, the contribution of the previous reaction is neglected in the inert atmosphere as has been shown by Miller et al. [23].

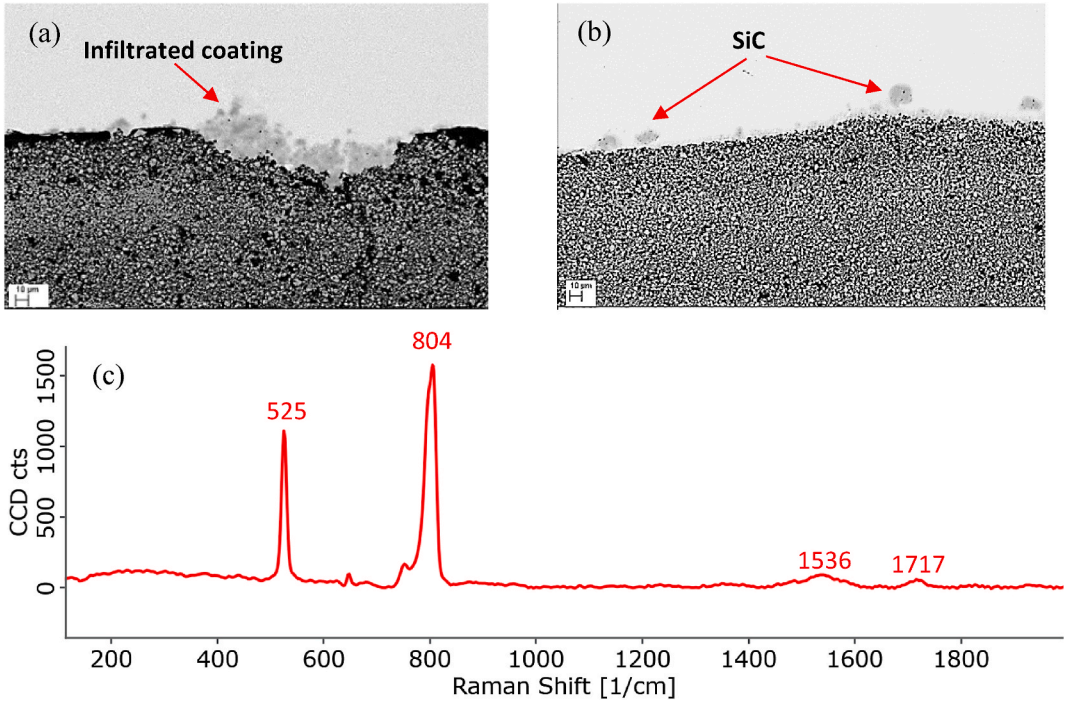

Fig. 11. Liquid-coating interface after 30 min holding at 1723 K of (a) substrate coated with coating-B, and (b) substrate coated with coating-A. (c) Raman spectrum of a SiC particle at the liquid interface that is shown in (b).

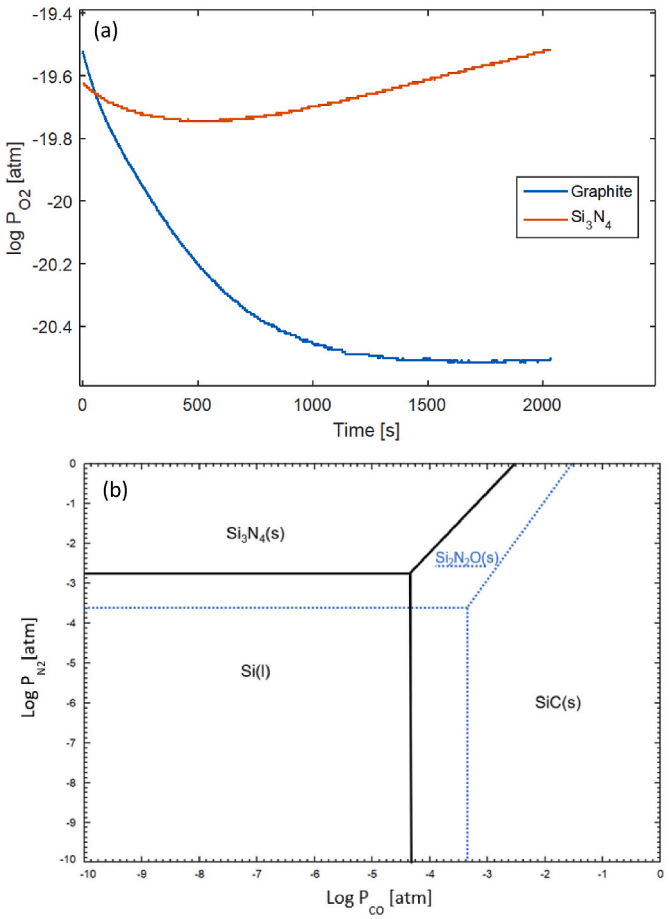

Fig. 12. (a) Oxygen evolution during silicon melting on two different substrates under the same coating and melting conditions. (b) Phase stability diagram[11] of Si–O–N–C system at 1723 for two oxygen partial pressure logarithmic values: −19 (blue-dotted line) and −21 (black solid line). Detailed diagrams are given in Supplementary materials at oxygen partial pressure of 10^{-19}-10^{-21} atm. (For interpretation of the references to color in this figure legend, the reader is referred to the Web version of this article.)

Furthermore, in our work, no deoxidation of the coating is noticed at the coating-SiC interface as can be seen in Fig. 10. The impact of SiC on silica reduction is considered to be negligible as the resultant partial pressure of CO is lower by three orders of magnitude than in the case of carbon [13]. On the other hand, Si_3N_4 and SiC can coexist together without any interactions as reported by many previous studies [24,25], and agrees with the results in this work. Furthermore, no degradation of the coating is noticed at the coating-substrate interface of types D and E as can be seen in Fig. 13 and Fig. 14.

3.4. Interactions at the liquid-coating interface

Two major factors contribute to the intermediate layer formation at the coating-liquid interface: i) the direct dissolution of the coating particles in the melt, and ii) the dissolution of product gases that diffuse from the coating-graphite interface and the bulk coating to the liquid. The interactions between the liquid and silicon nitride particles have been studied previously by Ref. [5] for coated quartz crucibles. However, in the case of graphite substrates, it is essential to consider the evolution of product gases from the coating-substrate interface and their effect on the chemistry of the melt-coating interface. The main detrimental gas is CO as it reacts with the liquid and forms SiC particles at the liquid front because of the melt saturation of carbon. The main sources of CO gas in the system are:

i. The reaction between SiO gas and graphite insulation, which is considered a common source in the crystallization of silicon since the industrial furnaces are graphite insulated.
ii. The reaction between graphite and SiO_2 in the coating, which occurs when the silica has direct contact with the graphite as in a one-layer configuration. This source can be eliminated by applying a protective layer of porous coating, namely types B, D, E, or dense SiC layer as in coating type-C.
iii. The reaction between SiO gas and the graphite substrate. SiO diffuses through the porous coating and reacts with graphite. This reaction is avoided by depositing a dense silicon carbide layer at the graphite surface as in Coating-C.

Fig. 11 shows the liquid-coating interface of two coating configurations. Less SiC precipitation is observed in the two-layer configuration as seen in Fig. 11 a. Some silicon carbide particles were formed at the liquid front of one-layer coated samples as shown in Fig. 11 b and confirmed by Raman spectrum in Fig. 11.c whereas the peaks 805, 525 and 752 cm −1 correspond to the formation of crystalline SiC [22]. The careful examination of the liquid-coating interface for the five coating methods reveals that SiC is mainly formed in the samples coated by method A. Therefore, it seems that the second source of CO has a major contribution to the melt contamination by carbon. This observation agrees with the continuous SiC layer that has been reported recently by Camel et al. [2] at the liquid-coating interface of G1 ingots, which were directly coated with an oxidized silicon nitride layer. It has been shown by Ref. [5] that this layer, at the liquid interface, facilitates the ingot removal and also prevents liquid infiltration during melting. But the carbon concentration profiles in Ref. [2] reveal a high level of carbon in the melt, which approaches the saturation limit. Thus, applying coating A can be advantageous in terms of simplicity and effectiveness as a non-sticking coating while the high level of CO is challenging. One feasible solution can be increasing the argon flow rate during the directional solidification. However, this will negatively affect the coating stability by accelerating the SiO_2 dissociation.

3.5. Phase stability in Si–N–O–C system

Fig. 12.a shows the oxygen evolution in the furnace during in-situ experiments of silicon nitride and graphite substrates. It is noteworthy that the same coating and melting conditions are applied on both substrates. Yet, lower oxygen partial pressure values are obtained with graphite substrates compared with silicon nitride substrates. The Si–N–O–C phase stability diagram in Fig. 12.b is calculated at two oxygen partial pressure values: 10^{-19} and 10^{-21} atm, which were selected based on the experimentally measured values of oxygen partial pressure in the furnace with a tolerance of $10^{\cdot.5}$ atm on the upper and the lower limits. As can be noticed in the phase diagram, the stability of silicon oxynitride degrades severely as the oxygen partial pressure decreases in the furnace atmosphere. This explains the faster transition in the coating behavior from de-wetting to wetting conditions of graphite substrates compared with the wetting behavior of Si_3N_4 substrates, which have been reported in Ref. [14]. Consequently, the dissociation of silicon oxynitride at the liquid front promotes liquid infiltration and spreading Ref. [14].

To better understand the contribution of each substrate material, we measured the oxygen evolution in the furnace under the same heating and argon flow profile before each experiment. These measurements are considered as background measurements for the oxygen values to eliminate the influence of the oxygen traces that might exist in the argon gas source. Despite the higher deoxidation rates of coated graphite substrates, the oxygen profiles after the background subtraction reveal a lower oxygen evolution rate with graphite compared with Si_3N_4 (see Fig. S5. in Supplementary Materials).

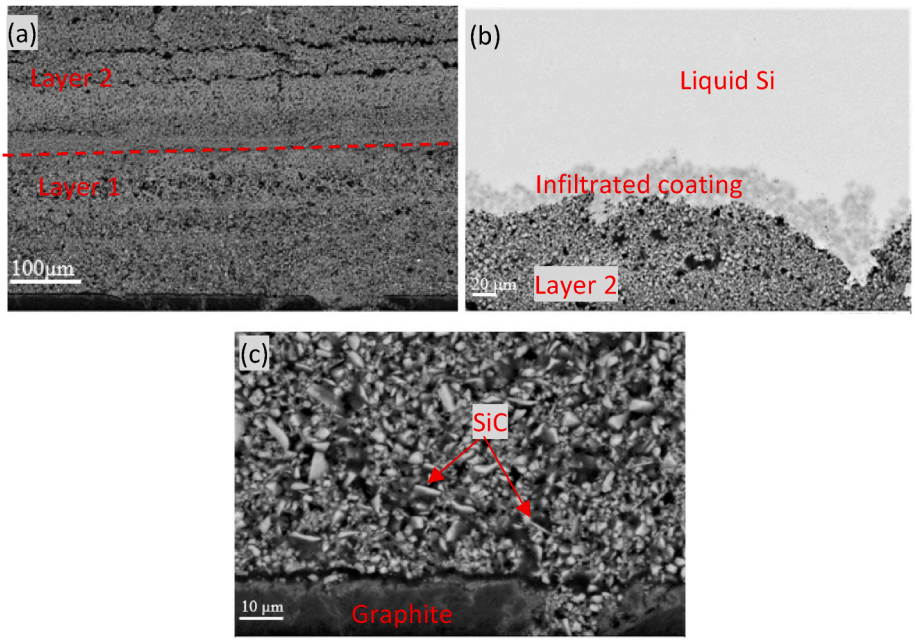

Fig. 13. Two-layer type-E coating microstructure after in-situ melting for 50 min at 1723 K. (a) the first layer is Si_3N_4+ SiC, the second layer is Si_3N_4 + SiO_2. (b) Coating-liquid interface, (c) coating-substrate interface, the needle-shaped particles are SiC. The initial oxygen mass concentration of the top layer is 8 wt.%. The total coating thickness is 400 μm.

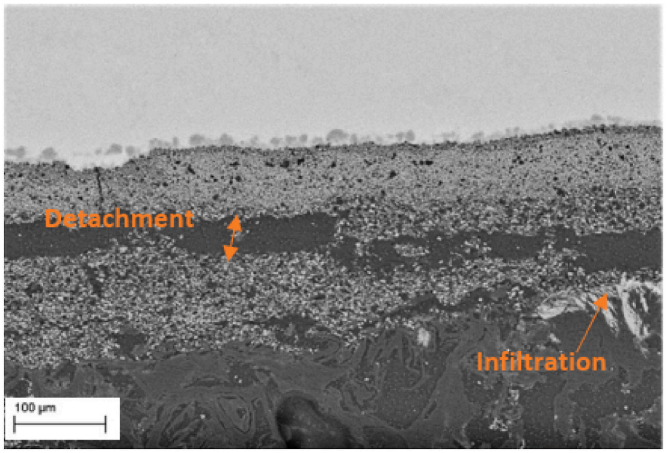

Fig. 14. Detachment of the first layer of Coating-D during melting. The bottom layer is a porous SiC coating layer, and the top layer is Si_3N_4 + SiO_2. The initial oxygen mass concentration of the top layer is 8 wt.%. The coating thickness is approximately 200 μm.

3.6. Discussions on coatings for graphite-use in PV Si applications

The two-layer coatings, Coatings B-E, are proposed to prevent the detrimental reactions in the graphite-silicon system. The primary goal of the coatings is to avoid silicon infiltration into the substrate and minimize the detrimental interaction between graphite and SiO_2. The solutions that have been reported in the literature are either lining the graphite crucibles interior with a dense SiC layer [13] or applying a thick oxidized silicon nitride layer directly on the graphite material [2]. The deposition of a dense silicon carbide layer by silicon infiltration on the graphite surface, Coating C, is a viable solution that will hinder the reaction between SiO_2 and graphite and decrease the CO evolution in the furnace. However, it is worth noting that the thickness of this layer cannot be controlled. This results in a non-uniform thickness layer as well as formation of silicon carbide at various depths in the graphite crucible. The thermal expansion coefficient mismatch between graphite and SiC should be carefully considered if this method is selected as it can induce stresses [21] in the crucibles under cyclic heating and cooling and reduce their lifetime. The second solution implies that the graphite will react with the SiO_2 content and develop CO gas in the melt, which in turn will form a SiC layer at the liquid-coating interface. This solution might be practical but at the expense of ingot purity. SiC precipitates will not only affect the final quality of silicon ingots but also the efficiency of diamond wire wafering of the silicon ingots [27]. In our study, we tackled this challenge by applying two-layer coating methods that combine the de-wetting properties and protection of the graphite materials. The reaction between graphite and silicon nitride is beneficial for these crucibles as a silicon carbide layer will form during the use without the evolution of CO gas. Coatings B, D, and E imply the same concept of depositing a porous layer below the oxidized silicon nitride top layer. Fig. 13.a shows the microstructure of coating E, which has a porous Si_3N_4: SiC layer deposited on the graphite surface. As shown in Fig. 13.b, no SiC particles are found at the liquid-coating interface, which indicates a low CO level and approves the potential of the bottom layer as a protective layer. The addition of SiC to the first layer enhances the adhesion between both layers as well as the adhesion on the graphite surface. Moreover, the needle-shaped SiC particles develop a higher cohesive strength within the first layer, which decreases the risk of cracking during melting as observed in Fig. 13.c. The resulting cohesive microstructure of coating-E positively impacts the liquid de-wetting behavior, which is comparable to the wetting behavior of method-B. Fig. 14 illustrates some challenges with Coating-D as it experiences cracking within the first layer and detachment from the second layer. The cracks in the porous SiC layer accelerate the liquid infiltration towards the graphite substrates.

4. Conclusions

The utilization of graphite materials in the PV Si applications needs careful consideration of the interaction that takes place between the

[1] Calculated by Factsage 8.1.

graphite and the coating components, which can negatively affect the quality of crystallized silicon ingots. In this study, we suggested different coating configurations that can be applied to the reusable graphite crucibles for PV Si applications. The best de-wetting conditions are achieved by coating the graphite substrates with a two-layer method: (i) the first layer is a porous Si_3N_4 or Si_3N_4: SiC layer to suppress SiO_2-graphite interaction, (ii) the second layer is Si_3N_4 mixed with colloidal silica to improve the surface non-wetting properties. The optimal coating thickness of each layer is found experimentally within the range of 200 ± 50 μm, and thereby the optimum total thickness is within the range of 400 μm. The addition of SiC powder to the bottom layer enhances its cohesion as well as its adhesion to the top layer and the graphite substrate. One of the key benefits of the two-layer configurations is the formation of SiC as a product of the Si_3N_4-graphite reaction without the evolution of the harmful CO gas that contaminates the melt. Both methods (B and E) show minimal wetting rates compared with the other coating techniques especially at 8 wt.% of oxygen in the top layer, which is found as the optimal oxygen concentration.

The coated graphite substrates show the highest oxygen depletion rates during the isothermal holding in comparison with the reference silicon nitride and quartz substrates. Graphite acts as an additional driving force for SiO_2 reduction, as SiO gas diffuses through the porous coating and reacts with graphite substrate to produce CO gas. The evolution of CO results in the formation of silicon carbide particles at the coating-liquid interface. However, the CO effect is expected to decrease with an increasing number of uses of graphite crucibles as a protective SiC layer will form at the graphite surface.

CRediT authorship contribution statement

Rania Hendawi: Conceptualization, Methodology, Investigation, Formal analysis, Writing – original draft, Writing – review & editing. **Lars Arnberg:** Conceptualization, Supervision, Validation, Writing – review & editing. **Marisa Di Sabatino:** Conceptualization, Supervision, Validation, Writing – review & editing, Funding acquisition, Project administration.

Declaration of competing interest

The authors declare that they have no known competing financial interests or personal relationships that could have appeared to influence the work reported in this paper.

Acknowledgments

This work was performed within the project Crucibles for Next Generation High-Quality Silicon Solar Cells (CruGenSi), with contract number 268027 and funded by the Research Council of Norway and industry partners.

Appendix A. Supplementary data

Supplementary data to this article can be found online at https://doi.org/10.1016/j.solmat.2021.111422.

References

[1] M.P. Bellmann, G. Stokkan, A. Ciftja, J. Denafas, T. Kaden, Crystallization of multicrystalline silicon from reusable silicon nitride crucibles: material properties and solar cell efficiency, J. Cryst. Growth 504 (2018) 51–55.
[2] D. Camel, E. Cierniak, B. Drevet, R. Cabal, D. Ponthenier, N. Eustathopoulos, Directional solidification of photovoltaic silicon in re-useable graphite crucibles, Sol. Energy Mater. Sol. Cell. 215 (2020) 110637.
[3] C.K.a.F. Schmid, Reusable Crucible for Silicon Ingot Growth, Crystal Systems, Inc., USA, 2003.
[4] R. Hendawi, A. Ciftja, G. Stokkan, L. Arnberg, M. Di Sabatino, The effect of preliminary heat treatment on the durability of reaction bonded silicon nitride crucibles for solar cells applications, J. Cryst. Growth 542 (2020) 125670.
[5] D. Camel, B. Drevet, V. Brizé, F. Disdier, E. Cierniak, N. Eustathopoulos, The crucible/silicon interface in directional solidification of photovoltaic silicon, Acta Mater. 129 (2017) 415–427.
[6] B. Drevet, O. Pajani, N. Eustathopoulos, Wetting, infiltration and sticking phenomena in Si 3N 4 releasing coatings in the growth of photovoltaic silicon, Sol. Energy Mater. Sol. Cell. 94 (2010) 425–431.
[7] I. Brynjulfsen, A. Bakken, M. Tangstad, L. Arnberg, Influence of oxidation on the wetting behavior of liquid silicon on Si3N4-coated substrates, J. Cryst. Growth 312 (2010) 2404–2410.
[8] A. Casado, J. Torralba, S. Milenkovic, Wettability and Infiltration of Liquid Silicon on Graphite Substrates, 2019.
[9] A. Ciftja, T.A. Engh, M. Tangstad, Wetting properties of molten silicon with graphite materials, Metall. Mater. Trans. 41 (2010) 3183–3195.
[10] J.-G. Li, H. Hausner, Wetting and infiltration of graphite materials by molten silicon, Scripta Metall. Mater. 32 (1995) 377–382.
[11] J. Roger, G. Chollon, Mechanisms and kinetics during reactive infiltration of molten silicon in porous graphite, Ceram. Int. 45 (2019) 8690–8699.
[12] J. White, L. Ma, K. Forwald, D. Sichen, Reactions between silicon and graphite substrates at high temperature: in situ observations, Metall. Mater. Trans. B 45 (2013) 150–160.
[13] C. Huguet, C. Dechamp, D. Camel, B. Drevet, N. Eustathopoulos, Study of interactions between silicon and coated graphite for application to photovoltaic silicon processing, J. Mater. Sci. 54 (2019) 11546–11555.
[14] R. Hendawi, A. Ciftja, L. Arnberg, M. Di Sabatino, Kinetics of silicon nitride coatings degradation and its influence on liquid infiltration in PV silicon crystallization processes, Sol. Energy Mater. Sol. Cell. 230 (2021) 111190.
[15] P. Shen, H. Fujii, T. Matsumoto, K. Nogi, Reactive wetting of SiO2 substrates by molten Al, Metall. Mater. Trans. 35 (2004) 583–588.
[16] S. Deng, G. He, L. Wang, Q. Meng, Z. Yang, J. Li, L. Jiang, Combustion synthesis of Si2N2O powder for photovoltaic silicon casting application, Ceram. Int. 47 (2021) 5795–5802.
[17] Z. Yuan, W.L. Huang, K. Mukai, Wettability and reactivity of molten silicon with various substrates, Appl. Phys. A 78 (2004) 617–622.
[18] B. Drevet, R. Voytovych, R. Israel, N. Eustathopoulos, Wetting and adhesion of Si on Si3N4 and BN substrates, J. Eur. Ceram. Soc. 29 (2009) 2363–2367.
[19] N. Klinger, E.L. Strauss, K.L. Komarek, Reactions between silica and graphite, J. Am. Ceram. Soc. 49 (1966) 369–375.
[20] C. Huguet, C. Dechamp, R. Voytovych, B. Drevet, D. Camel, N. Eustathopoulos, Initial stages of silicon–crucible interactions in crystallisation of solar grade silicon: kinetics of coating infiltration, Acta Mater. 76 (2014) 151–167.
[21] M. Dragomir, M. Valant, M. Fanetti, Y. Mozharivskyj, A facile chemical method for the synthesis of 3C–SiC nanoflakes, RSC Adv. 6 (2016) 21795–21801.
[22] J.S. Oh, J. Lee, Kinetics of SiC formation on graphite using N2-CO-SiO and N2-CO-H2-SiO gas mixtures, Metall. Mater. Trans. B 50 (2019) 1808–1813.
[23] P.D. Miller, J.G. Lee, I.B. Cutler, The reduction of silica with carbon and silicon carbide, J. Am. Ceram. Soc. 62 (1979) 147–149.
[24] N. Kishan Reddy, Reaction-bonded silicon carbide refractories, Mater. Chem. Phys. 76 (2002) 78–81.
[25] S.N. Perevislov, D.D. Nesmelov, Properties of SiC and Si3N4 based composite ceramic with nanosize component, Glass Ceram. 73 (2016) 249–252.
[27] G. Du, L. Zhou, P. Rossetto, Y. Wan, Hard inclusions and their detrimental effects on the wire sawing process of multicrystalline silicon, Sol. Energy Mater. Sol. Cells 91 (2007) 1743–1748.